PAGEOPH, Vol. 141, No. 2/3/4 (1993) 0033-4553/93/040523-21$1.50 + 0.20/0

Improvements to Griggs-type Apparatus for Mechanical Testing at High Pressures and Temperatures

TRACY N. TINGLE,[1,3] HARRY W. GREEN, II,[1,4] THOMAS E. YOUNG[1] and TED A. KOCZYNSKI[2]

Abstract—New and improved techniques and apparatus for testing the mechanical properties of materials at high pressures and temperatures are described. These include an improved Griggs-type deformation apparatus designed to operate to 5 GPa and associated servo-controlled hydraulic drive and electronics, the design of hydrostatic (molten alkali halide mixtures) pressure assemblies to measure flow stresses as low as a few MPa, the characterization of temperature gradients and friction in such assemblies, measurement of the melting curve of an alkali halide mixture used as a confining pressure medium, and the measurement of acoustic emissions.

Key words: Pressure, temperature, stress, measurement, acoustic emissions, deformation, techniques.

Introduction

In recent years, the field of high-pressure experimental rock deformation has experienced several advances due to improvements in techniques and equipment. Some of the important advances include (i) development of hydrostatic pressure assemblies utilizing molten alkali halide confining media (GREEN and BORCH, 1989, 1990; GLEASON and TULLIS, 1992, 1993), (ii) measurement of low flow stresses (a few MPa) in such assemblies (BORCH and GREEN, 1989; MEAGHER *et al.*, 1992), (iii) monitoring of acoustic emissions (GREEN *et al.*, 1992; TINGLE *et al.*, 1993), and (iv) quasi-controlled deformation of materials at very high pressures in multianvil apparatus (GREEN *et al.*, 1990, 1992; GREEN and WALKER, 1992; BUSSOD *et al.*, 1992; WEIDNER *et al.*, 1992) and in diamond anvil cells (MEADE and JEANLOZ, 1990, 1991; WU *et al.*, 1993).

[1] Department of Geology, University of California, Davis, CA 95616, U.S.A.
[2] Rock Mechanics, Lamont-Doherty Earth Observatory, Palisades, NY 10984, U.S.A.
[3] Now at Department of Geological and Environmental Sciences, Stanford University, Stanford, CA 94305, U.S.A.
[4] Now at Department of Earth Sciences and Institute of Geophysics and Planetary Physics, University of California, Riverside, CA 92521-0412, U.S.A.

This paper describes new techniques and apparatus for axial deformation at strain rates of 10^{-2} to $10^{-7}\,s^{-1}$ in a Griggs-type apparatus, improvements in the design of such apparatus, and the measurement of acoustic emissions.

Experimental Apparatus

5 GPa Deformation Apparatus

Figure 1 depicts the new Griggs-type deformation apparatus. The load frame was designed to sustain confining pressures to 5 GPa, the practical upper limit for deformation imposed by the room-temperature compressive strength of the tungsten carbide (WC) deformation pistons. The maximum pressure at which specimens

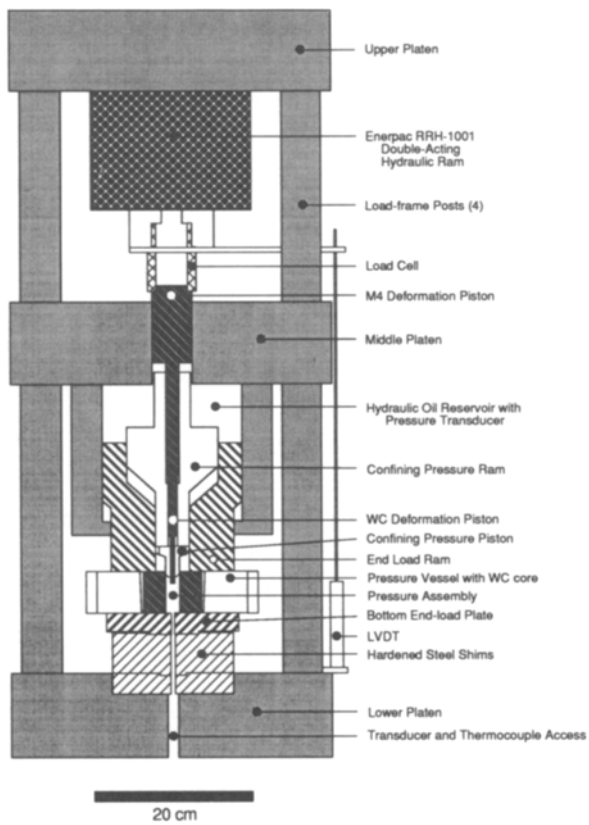

Figure 1
Schematic drawing of the 5 GPa load frame, confining pressure ram, hydraulic drive and standard pressure vessel. Note the axial hole in the lower platen and base plate used to introduce the acoustic transducer and additional thermocouples.

have been deformed in the new apparatus is 2800 MPa (TNT and HWG, unpublished results). Details of the new apparatus will be published after the end-load modifications for attainment of maximum pressure are completed (HWG and I. C. Getting, manuscript in preparation).

Data Collection and Analysis

Measurement of all experimental variables (pressure, load or stress, temperature, displacement, and acoustic emissions) is controlled by computer. Confining pressure is calculated from the oil pressure of the confining pressure hydraulic ram (Figure 1), as measured by a pressure transducer (Precise Sensors Model 6550). The axial force applied to the specimen is measured by a load cell between the deformation ram and pistons (Houston Scientific Model 3500; Figure 1). Temperature is measured by two type-B thermocouples adjacent to the specimen (Figure 2) and controlled by a Eurotherm Model 818P temperature controller interfaced (via an RS232 serial communications port) to the computer. This allows the temperature and power output of the controller to be monitored and stored on disk (all temperature controller functions are handled by the computer via the interface). Furnace power (1000–1600 W) is supplied through a 3 kVA AC power transformer (115:8) by a silicon-controlled rectifier (SCR) driven by the temperature controller. Displacement is measured by a linear voltage displacement transducer (LVDT; Schaevitz Model DC-E500).

Output voltages of the various transducers and thermocouples are measured by Omega OM3 series signal conditioners interfaced to analog-digital data acquisition and control boards internal to the computer (IBM-PS2 with IBM Data Acquisition and Control System). The resolution imposed by the 12-bit analog-digital converters corresponds to 1 MPa for the measured confining pressure and piston stress, 1 K for temperature, and 0.3 μm for displacement. Data acquisition is performed by FORTRAN programs written in our laboratory, and data are stored on disk for subsequent analysis. The data are subsequently transferred to Macintosh computers and stress-strain curves are calculated (described below) utilizing Kaleidagraph®, a software graphics and analysis package.

Pressure Assemblies

The high-pressure sample assemblies are designed to accommodate a diversity of experimental conditions (Figure 2). Changes can be made to the size of the specimen, the position of the specimen within the furnace, the position of the two thermocouples, the thicknesses of the furnace tube and ceramic sheaths, the length and composition of the metal sleeve (used to decrease the specimen temperature gradient), and the compositions of the alkali halide mixtures providing the confining pressure. Central holes in the lower platen and base plates provide access to

the pressure assembly, so that a piezoelectric transducer may be placed in close proximity to the base of the specimen to record acoustic emissions, or additional thermocouples may be positioned inside the volume normally occupied by the specimen (Figures 1, 2).

Figure 2a shows the standard configuration for moderate temperature (up to 1450 K) experiments. The graphite furnace tube is sandwiched between two cylin-

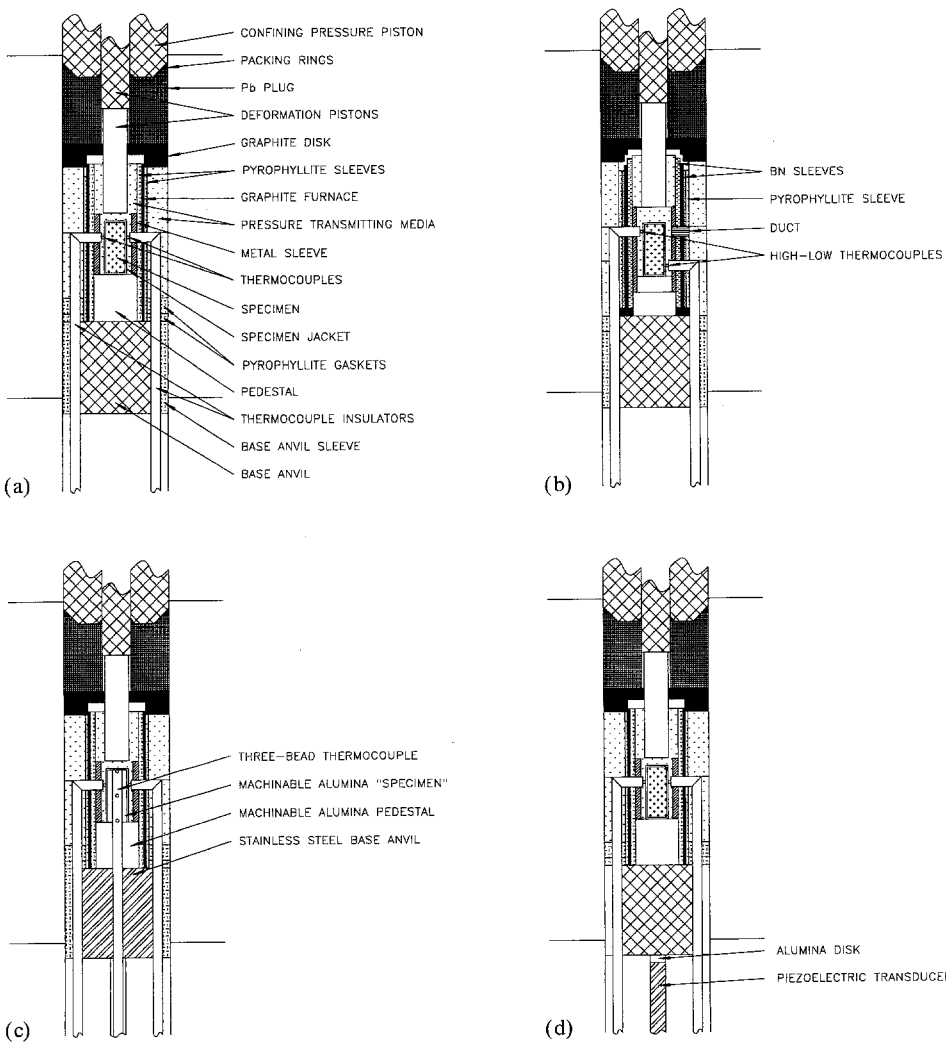

Figure 2

Schematic drawings of pressure assemblies used in the high-pressure deformation experiments. (a) Standard high-pressure assembly. (b) Assembly modified for temperatures above 1450 K. (c) Assembly for measuring temperature distribution. (d) Assembly used for acoustic emission experiments. Components and materials are labeled and indicated. For scale, the diameter of the assemblies is 1.75 cm.

ders of "soft-fired" pyrophyllite (Alsimag Technical Ceramics Machinable Grade A Lava, a natural material composed mostly of pyrophyllite, fired at 1223 K for 1 hr). The porous soft-fired pyrophyllite sleeves are able to compact during pressurization of the assembly, and they protect the furnace tube from damage due to traction imposed on the furnace assembly by the compacting outer salt sleeves. Pyrophyllite reacts to an aluminosilicate phase (mullite, andalusite, or kyanite depending on pressure) + quartz above 700 K (KERRICK, 1968 and references therein). At low pressures, the fired pyrophyllite probably melts incongruently at 1450–1500 K (DE VRIES, 1964); at 2520 MPa, HASKELL and DEVRIES (1964) report the kyanite + quartz eutectic to be 1450 K. Such melting can damage the graphite furnace, necessitating the use of a more refractory material (such as boron nitride or alumina) for long-term experiments at temperatures above 1500 K.

A metal sleeve fabricated from Inconel 600, Ni, or Mo is placed inside the inner ceramic sleeve to provide a more uniform temperature distribution near the specimen (Figure 2). Inconel and Ni have 1-bar melting temperatures of 1627–1686 and 1728 K, respectively (CRC Handbook of Materials Science; CRC Handbook of Chemistry and Physics). However, at moderate pressures (<2 GPa) and temperatures above 1450 K, both metals dissolve extensively in the molten salts, which leads to alloying and embrittlement of the Pt specimen jacket and metal precipitation in the cooler regions of the molten volume. Mo is used above 1450 K because of its high melting temperature (2883 K at 1 bar, CRC Handbook of Chemistry and Physics) and resistance to reaction and dissolution in the molten salts. However, its cost and the difficulty of machining limit the desirability of Mo for use in all experiments. GLEASON and TULLIS (1993) employed a graphite sleeve as a thermal conductor in their 2.54 cm high-pressure molten salt assembly.

Two type-B ($Pt_{94}Rh_6$-$Pt_{70}Rh_{30}$) thermocouples in ceramic thermocouple sheaths are placed in direct contact with the Pt specimen jacket. The thermocouples are inserted through holes in the ceramic, graphite, and metal sleeves. Where the thermocouples penetrate the sleeves (Figure 2), sintered high-purity alumina (McDanel's $>99.5\%$ Al_2O_3) is used as the sheath material to minimize chemical contamination of the thermocouple bead. Outside the furnace in the lower-temperature region, mullite is used because it compacts and collapses around the thermocouple wires and prevents extrusion of the molten salt confining pressure medium. An unfired pyrophyllite gasket is placed at the top of the "hard-fired" (1423 K for 1 hr) pyrophyllite base-anvil sleeve to prevent the sheaths from being extruded. The thermocouple wires are glued (Zircar® alumina cement) into the sheaths, and the sheath is glued into the base anvil sleeve to further prevent extrusion and "blow-outs." The tips of the thermocouples also are coated with Zircar®.

The Pt-encapsulated specimen is cast into the metal sleeve with the desired alkali halide confining-pressure medium using a micro-oxy-acetylene torch and special jigs for aligning the specimen. The cast specimen and metal sleeve rest on a sintered alumina pedestal, which in turn rests on a WC (Federal grade FC-3) base anvil

(Figure 2). The base anvil serves as an electrical lead for the graphite furnace and is sleeved in hard-fired pyrophyllite to insulate the anvil from the pressure vessel, which serves as the other lead. A sintered alumina deformation piston is situated above the specimen. This piston is pushed by a movable WC piston that enters the high-pressure volume through an axial hole in the confining pressure piston (Figure 1). The WC piston enters through an Al-bronze 600 packing ring and a Pb plug at the top of the assembly. The alumina piston moves through the Pb plug and graphite disk, which are intended to distribute the force from the confining pressure piston evenly to the various components of the pressure assembly and the inner salt (which may be solid or molten around the specimen, depending upon the requirements of the experiment). The graphite disk also serves as the electrical contact between the furnace tube and the pressure vessel.

The salt outside the furnace is KCl or NaCl, hydrostatically cold-pressed to 200 MPa in an evacuated rubber bladder placed in a large-bore (5 cm) pressure vessel filled with hydraulic fluid, and machined to final dimensions. The composition of the inner salt is NaCl, the 1-bar NaCl-KCl eutectic, or the lowest-melting 1-bar eutectic in the K-Na-Ca-Ba-Cl system (referred to hereafter as E4; LEVIN *et al.*, 1969). The inner salt is cast around the specimen in the metal sleeve as described above. The same salt mixture is cast around the alumina piston above the specimen, or a separate piece is isostatically cold-pressed to final dimensions in a special hardened steel jig. For most experiments, the composition of the inner salt is chosen to produce melting around the specimen and extensive, but not complete, melting above it. Thus, for relatively low temperature experiments (800–1400 K), the E4 mixture is used, whereas for temperatures above 1400 K, NaCl or the KCl-NaCl eutectic mixture is used. For high-stress experiments (>600 MPa), a solid salt must be used to avoid axial splitting of the alumina piston. The outer salt (NaCl or KCl) is chosen so that little, if any, melt is produced. KCl is generally used below 1500 MPa, and NaCl is used above 1500 MPa; the KCl I–II phase transition at ~ 1800 MPa (CLARK, 1959) may cause some anomalous compaction problems that lead to furnace damage.

Figure 2b shows some modifications that have been made to increase high-temperature furnace life and to improve knowledge of the temperature profile during deformation. The material of the sleeves adjacent to the graphite furnace is boron nitride (Union Carbide HBR-grade BN), which has a much higher melting temperature than pyrophyllite. Additionally, BN alters the chemical environment inside the furnace such that the Mo sleeve does not react or dissolve in the molten salt. A pyrophyllite sleeve is used outside of the outer BN sleeve to provide mechanical protection to the brittle and relatively weak BN during pressurization. The BN, in turn, protects the graphite furnace from pyrophyllite melting at high temperatures. To further protect the sleeves and furnace from damage during pressurization, a graphite ring is placed at the base of the sleeves for "cushioning."

For most experiments, the thermocouples are placed in a high-low arrangement to deduce the specimen temperature profile (the true temperature distribution is a complicated function of the exact placement and length of all the components and their thermal diffusivities, the amount of power being applied to the furnace, and numerous other variables). The temperature profile can change with time during an experiment due to movement of the deformation piston and, at very high temperatures, due to convection of the molten salt and degradation of the furnace with time at temperature. Experiments performed with the purpose of determining the temperature distribution are described in a later section.

A ceramic duct (sintered alumina four-hole thermocouple tube) is placed opposite the upper thermocouple to provide a conduit for equalization of pressure between the inner and outer salt volumes during advancement and retraction of the deformation piston. It is intended to avoid over- or underpressurizing the inner volume, which can lead to fracture of the furnace and ceramic sleeves.

Servo-controlled Hydraulic Drive

A servo-controlled hydraulic drive, similar to that developed by SCHOLZ and KOCZYNSKI (1979), was installed on the new apparatus prior to performing the acoustic emissions tests (described below) in order to eliminate mechanical noise inherent in a gear train driven by a stepping-motor. However, there are other advantages to such a system, including ease of operation and precise control of the deformation piston based on either the measured displacement or load.

The deformation pistons are advanced and retracted by a double-acting hydraulic cylinder (Enerpac RRH-1001) controlled by an electro-hydraulic servo-controller monitoring either the LVDT (displacement feedback) or the load cell (load feedback) to close the servo loop. The double-acting hydraulic ram is driven by a Vickers (Model TK20, 20 MPa, 19 L min^{-1}) hydraulic pump and accumulator. The servo-controller also is interfaced to the computer, thus providing a fail-safe (in addition to those built into the servo) in the event of power or furnace failure and the capability to automate and program the deformation cycles. Additional details about the servo-controlled hydraulic drive system can be found in SCHOLZ and KOCZYNSKI (1979). Preliminary experiments suggest that it will be feasible to conduct creep (constant stress) tests with the hydraulic drive, although systematic exploration has not yet been undertaken.

Characterization of Friction on the Deformation Pistons

The strength of the specimen is measured external to the high-pressure volume (Figure 1). Hence, the measured stresses necessarily include forces acting on the deformation pistons other than those imposed by the mechanical strength of the

specimen. In this and subsequent discussions, these additional forces are referred to as "friction;" in fact, some of them are viscous.

Forces acting on the deformation pistons include (i) friction on the deformation piston packing ring, (ii) friction between the WC deformation piston and Pb plug, (iii) friction between the alumina deformation pistons and the Pb plug, (iv) friction between the alumina piston and the graphite disk used to make the upper furnace contact, (v) friction between the alumina piston and solid salt in the upper, colder, part of the furnace, (vi) viscous drag between the alumina piston and molten salt in the high-temperature region, (vii) the viscosity of the molten salt between the sample and the alumina piston, and (viii) the ductile strength of the lid of the Pt capsule. For experiments performed at constant piston-displacement rate or constant strain rate, as is the usual practice in our laboratory, these forces are either independent of or vary smoothly as a function of piston displacement (or time). The contribution of these additional forces to the measured stress is determined for each deformation cycle as described below.

At the start of an experiment, the WC and alumina deformation pistons are in direct contact (no Pb between them), and the alumina piston is 1–2 mm from the specimen. The abrupt rise in force when the alumina piston encounters the specimen establishes the onset of the deformation cycle (see Figures 9, 10), referred to later as the "hit-point." The confining pressure increases as the deformation piston advances. The contribution of the increased confining pressure to the measured stress is accounted for by subtracting the measured confining pressure from the piston stress, and the result is referred to as the "differential piston stress." The confining pressure measured during a deformation cycle also is subject to uncertainties due to friction between the confining pressure piston and packing ring and the finite strength of the confining pressure media. The steady advance of the deformation piston causes slow, steady retraction of the confining pressure piston. Hence the experiments correspond to the "hot piston-out" technique, and uncertainties in the measured pressure are typically less than 5% (e.g., JOHANNES *et al.*, 1971; MIRWALD *et al.*, 1975; HOLLAND, 1980). The differential piston stress is observed to be approximately constant or to increase slightly with piston displacement before the specimen is contacted. The differential piston stress measured immediately prior to the hit-point is assumed to represent the total friction on the deformation pistons throughout the cycle. Reduction of data showing attainment of steady-state flow at high temperatures confirms the general validity of this procedure (see Figure 10). In some cases, the change of total friction with displacement (time) is not trivial (with respect to the specimen strength), and a linear or quadratic fit to the pre-hit force record is extrapolated through the cycle and subtracted from the differential piston stress to obtain the stress on the specimen (see Figure 9).

If friction is not constant or varying slowly before specimen contact, significant uncertainties may be introduced into the stress measurements, and the data are

discarded because it generally signifies internal problems. For example, when the alumina deformation piston is in contact with the specimen, and Pb is present between the WC and alumina pistons, the differential piston stress may increase dramatically during piston advance. Moreover, the differential piston stress measured prior to the hit-point does not include the friction which must develop when that alumina piston begins to move and deformation of the sample begins. There is no way to deconvolve the friction on the alumina piston from the measured stress, and the data provide only an upper bound on the specimen strength. It is this effect that has introduced large systematic overestimates of strengths in previous studies with Griggs apparatus in which solid confining media were used (GREEN, 1992; GLEASON and TULLIS, 1992, 1993).

A number of modifications to the pressure assemblies have decreased the total friction. These improvements include using Al-bronze 600 (instead of mild or stainless steel) packing rings, replacing the upper salt wafer of the original molten salt assembly described by GREEN and BORCH (1989, 1990) with graphite, and utilizing lower-melting temperature alkali halide mixtures, thereby decreasing the amount of solid salt in contact with the alumina deformation piston. The absolute level of friction is of some concern because it does limit the maximum pressure at which deformation experiments can be performed.

Figure 3 compares the differential piston stress as a function of piston displacement measured at 500, 1000 and 1500 MPa confining pressure for Al-bronze 600 versus mild steel packing rings. The bore of the pressure vessel was filled with Pb and contained an axial 4 mm diameter alumina piston as in the standard pressure assemblies. As expected, the differential piston stress (total friction) increases with increasing confining pressure. However, the total friction is ~ 100 MPa lower in the experiments utilizing the Al-bronze packing rings. The total friction in the experi-

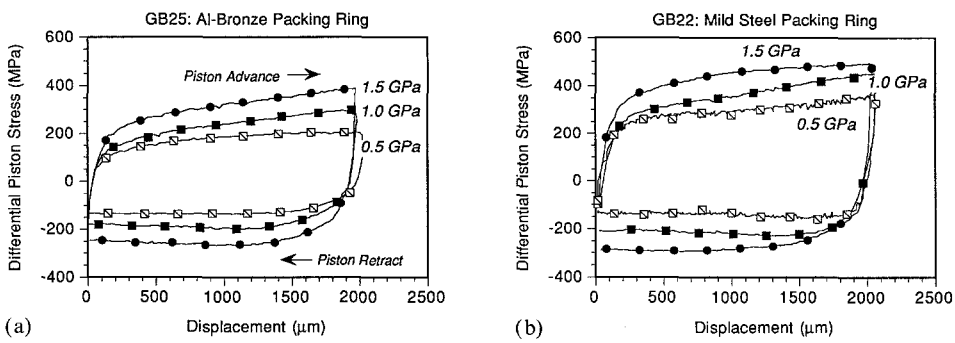

Figure 3

Differential piston stress-displacement data for experiments utilizing (a) an Al-bronze packing ring on the WC deformation piston (GB25) and (b) a mild steel packing ring (GB22). The data for each piston advance and retraction cycle are indicated: 0.5 GPa (square with diagonal), 1.0 GPa (solid square), and 1.5 GPa (solid circles); symbols were plotted every 10th data point.

ments above (Figure 3) is comparable to that measured in actual deformation experiments performed at high temperatures with molten and solid salt present. Although there are significant differences between these experiments and the deformation experiments, the data suggest that the friction exerted by the packing rings and Pb on the WC piston is the dominant source of friction in these high-pressure assemblies. The Al-bronze packing rings have been used successfully to a confining pressure of 2800 MPa.

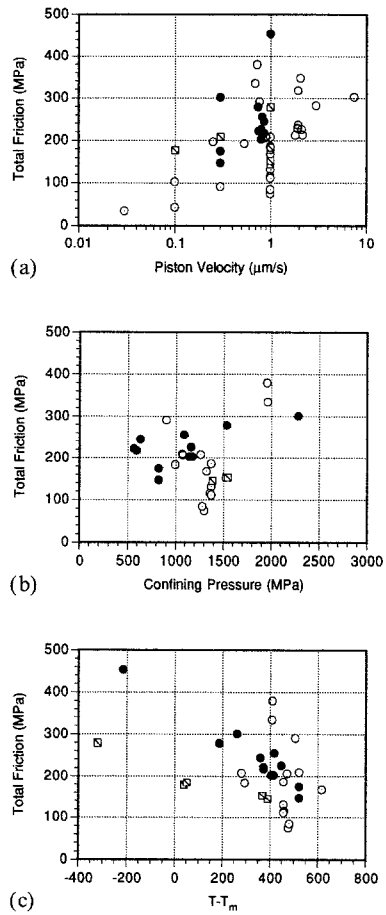

Figure 4

Total friction (differential piston stress at the hit-point) as a function of (a) piston displacement rate, (b) confining pressure for piston displacement rates in the range 0.8–1.2 μm s^{-1} and (c) specimen temperature relative to the melting temperature of the inner alkali halide mixture ($T - T_m$) for piston displacement rates in the range 0.8–1.2 μm s^{-1}. Symbols represent pressure assemblies (see Figure 2) utilizing the following: (1) upper NaCl disk, pyrophyllite inner furnace sleeve, and E4 inner salt (open circles), (2) upper graphite disk, pyrophyllite inner furnace sleeve, and E4 inner salt (solid circles), (3) upper graphite disk, BN inner furnace sleeve, and E4 inner salt (open circle and dot), (4) graphite disk, pyrophyllite inner furnace sleeve, and NaCl-KCl eutectic inner salt (square with diagonal).

The use of a graphite disk in place of the NaCl disk utilized in previous assemblies (GREEN and BORCH, 1989, 1990) reduced the differential piston stress (friction) by approximately 40–60 MPa, with a greater reduction noted at higher confining pressure (Figure 4). The total friction depends on the confining pressure, piston displacement rate, temperature, and details of the specimen assembly (Figure 4). Temperature is important because it determines the volume fraction of molten salt present; a higher volume of molten salt reduces the total friction. It has been our experience that the best results in multiple strain cycle experiments are obtained when the sample temperature is >200 K above the melting temperature of the alkali halide confining-pressure medium inside the graphite furnace. This decreases the contact area between solid salt and the alumina piston and helps ensure that the WC and alumina pistons remain in contact throughout the experiment. If the friction on the alumina piston is too high, Pb intrudes between the two pistons during retraction of the WC piston between deformation cycles. If one desires to perform multiple strain cycles (as are needed to precisely measure the stress exponent or activation energy), the presence of Pb between the two pistons introduces significant uncertainties to the stress measurement, as discussed above. Similarly, the composition of the furnace sleeves is important because if affects the thermal properties of the assemblies. Note that experiments using BN inner furnace sleeves exhibit lower friction than experiments using pyrophyllite sleeves. This probably is due to the much higher thermal diffusivity of BN (relative to pyrophyllite), and hence, greater volume of molten salt present during the experiment.

Measurement of Temperature Gradients

The mechanical behavior of many materials is a sensitive function of temperature. This is particularly true for partially molten materials, such as peridotite, in which the volume fraction of partial melt, and hence the mode of deformation and its effective flow stress, may change dramatically as a function of temperature.

The temperature distribution of the pressure assembly depicted in Figure 2c was characterized as follows: A single four-hole alumina thermocouple tube was used to sheath three type-B thermocouples whose beads were spaced approximately 2–3 mm apart. The stiffer $Pt_{70}Rh_{30}$ wire was used as the common reference wire for the three-thermocouple device. The thermocouple beads were covered with Zircar® alumina cement to inhibit contamination and extrusion of the molten NaCl pressure medium (although see discussion below). The sintered alumina pedestal was replaced by a crushable alumina cylinder with a hole to accommodate the thermocouples and sheath. A Pt capsule with the same dimensions as those used normally in our experiments was fitted around a hollow cylinder of alumina, and the three thermocouples were placed inside. Opposing thermocouples that touched the side of the Pt can were also present, for a total of five thermocouples inside the high-pressure, high-temperature volume. Thermoelectric potential was measured by

Omega OM3-ITC-B modules (linearized type-B thermocouple inputs) calibrated by a millivolt potentiometer source.

Figure 5 shows the measured temperatures for experiment GB41 relative to the controlling thermocouple. The temperature was ramped at 5 K min^{-1} to 1600 K. The perturbation in temperature recorded by the left (opposing), middle and bottom thermocouples at ~1350 K is perhaps due to melting and the onset of convection in the molten NaCl pressure medium inside the furnace. In experiment GB39 (not shown), melting of the salt (and the associated volume expansion on melting) caused a rupture in the graphite furnace, and the temperature difference increased dramatically to a maximum of −60 to −80 K relative to the control thermocouple, demonstrating the importance of maintaining the integrity of the graphite tube furnace for minimizing the temperature gradient in all high-pressure assemblies. In two experiments, one or more of the central thermocouples failed at 1450–1550 K due to extrusion of molten NaCl into the holes in the sheath for the thermocouple wires. The extrusion stretched and ultimately broke the Pt wires (as discussed above, the sintered alumina thermocouple tubes generally do not collapse around the thermocouple wires and alumina cement is generally not effective at preventing such "blow-outs"). This problem is unique to this particular assembly and is not a general problem for deformation or annealing experiments.

Figure 6 is a compilation of the data from three experiments (GB39, GB41 and GB43); the dashed curve is a second-order polynomial regression of those data. The "hot-spot" is located just slightly below the midpoint in the furnace. The maximum temperature difference in the region occupied by the sample is relatively small (±15 K at 1200 and ±20 K at 1500 K), corresponding to axial temperature

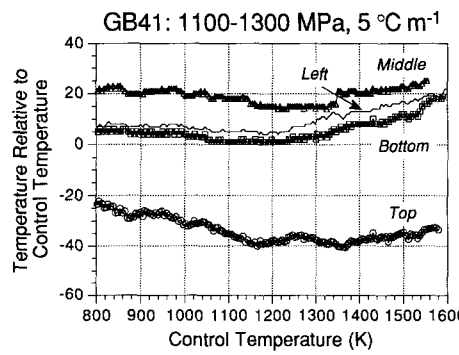

Figure 5

Thermal gradient measurement (experiment GB41) heated at a rate of 5 K min^{-1} at a confining pressure of 1100–1300 MPa (confining pressure increased during heating due to thermal expansion of the pressure assembly components). Upper (open circles), middle (open triangles), bottom (open squares) and left (solid line) thermocouple temperature are plotted relative to the control thermocouple (right thermocouple). The perturbation in the left and middle thermocouples at 1350 K may be due to the onset of melting of the NaCl confining pressure medium.

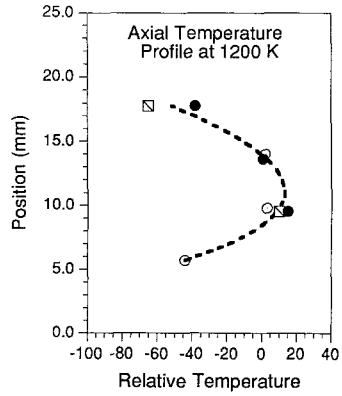

Figure 6

Axial temperatures, measured at 1200 K for experiments GB39 (squares with diagonal), GB41 (solid circles), and GB43 (open circles), plotted as a function of position in the graphite furnace. Thermocouple positions were varied by changing the height of the lower alumina base anvil, and hence the position of the Pt capsule; the position of the left and right control thermocouples remained fixed at a height of 13.6 mm. The maximum temperature difference at 1200 K over the length of an 8 mm specimen is estimated to be ± 15 K; the base of the specimen would be at a height of 7.62 mm. The furnace hot-spot is located slightly below the centerline of the furnace, probably because the assembly is not vertically symmetric and the thermal diffusivities of the various components are different.

gradients of $\pm 3-5$ K mm^{-1}. Lengthening the furnace will further reduce the axial temperature gradient, and this modification is in progress.

Thermal Analysis of Melting of the Alkali Halide Confining Pressure Medium

A number of alkali halide mixtures are utilized as confining pressure media. In particular, the E4 mixture is used frequently, because it possesses a very low melting temperature (700 K) at 1 bar, and it does not extensively dissolve the metal sleeves. Phase relations of these two-, three- and four-phase mixtures are well-known at 1 bar, but most have not been determined at higher pressures.

When the alkali halide confining-pressure medium begins to melt, it is expected that the furnace power will increase to provide the latent heat of fusion. KANZAKI (1990) used this heating curve method to detect melting of Au in a multianvil apparatus. By monitoring the temperature and furnace power closely while heating at a constant rate, it is possible to detect "plateaus" in the temperature-power curves due to the latent heat effects.

Figure 7 shows a well-developed thermal plateau at 935 K that is interpreted to represent first melting of the E4 salt. The melting curve of the E4 salt determined in this way from several experiments is shown in Figure 8. The data were fitted to the Simon equation ($P - P_0 = A[(T/T_0)^c - 1]$; CLARK, 1959), where $P_0 = 0$ and $T_0 = 700$ K. The best-fit parameters were determined to be A = 1636.7 and

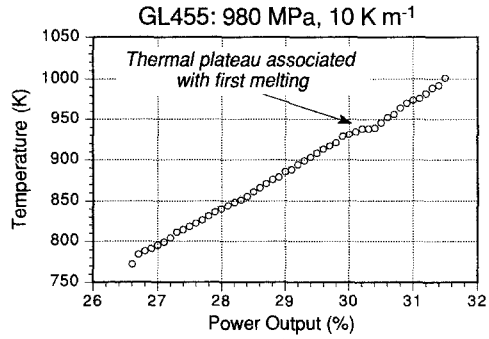

Figure 7

Temperature of the control thermocouple versus power output of the temperature controller to the SCR and the graphite furnace for experiment GL455 (980 MPa confining pressure and 10 K min^{-1} heating rate). The thermal plateau associated with the first melting of the E4 inner salt is indicated by an arrow. Increased power consumption at the melting point is due to the latent heat of fusion.

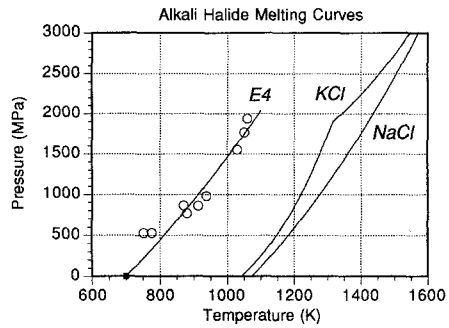

Figure 8

Data obtained by the heating curve method (Figure 7) for the melting of the E4 alkali halide mixture. The black square is the 1 bar eutectic (700 K) in the Na-K-Ca-Ba-Cl system (Figure 3320, LEVIN *et al.*, 1969). The melting curve calculated by the Simon equation (described in the text) is shown as a solid line. The melting curves for KCl and NaCl (CLARK, 1959) are shown for comparison.

$c = 1.788$, where P and T are in MPa and K, respectively. The observed scatter in these data may represent actual deviations in the melting behavior due to changes in the liquidus phase relations, or errors associated with salt preparation, determining the melting temperature from the thermal plateaus, or calibration of the confining pressure.

Measurement of Very Low Flow Stresses

It is possible to measure flow stresses as low as 3–5 MPa at high pressures and temperatures in the molten-salt pressure assemblies described here. This capability

was developed as part of our ongoing investigations into the rheology of partially molten peridotite and polycrystalline Ni (MEAGHER *et al.*, 1992). The procedures for making such measurements are described below.

The "zeroth-hit" procedure of GREEN and BORCH (1990) is used in low-stress experiments to (i) ensure that no Pb is present between the alumina and WC deformation pistons, (ii) flatten the lid of the Pt capsule, if present, and (ii) to locate the hit-point precisely. Commonly, the zeroth-hit is performed at 1200–1300 K at a strain rate of 10^{-4} s^{-1} (piston displacement rate of 1–2 μm s^{-1}). After loading the specimen elastically to a specimen stress of 200–400 MPa, the piston is retracted 1–2 mm, and the piston stress is monitored closely to determine if Pb has intruded between the alumina and WC pistons. If Pb does not intrude between the two pistons, the piston stress will decrease rapidly and remain constant at a differential piston stress comparable in magnitude (but negative) to that noted during piston advance. If Pb does intrude, the piston stress will increase 30–80 MPa within a few seconds after the specimen is unloaded, and the procedure above is repeated at a slightly higher temperature (+50 K) or to a slightly higher stress. After retracting both pistons intact, the temperature is increased to the desired value, and the low-stress deformation cycle begins.

Figure 9 shows the differential piston stress-displacement record for deformation of a partially molten synthetic pyrolite polycrystal ($\sim$5% partial melt) at 1090 MPa confining pressure, 1500 K, at a strain rate of 1.4×10^{-5} s^{-1} (experiment GB40). In this particular experiment, the hit-point was determined from the previous deformation cycle to be $\sim$8600 μm.

The raw data were smoothed by 100-point averaging to reveal the actual hit-point (Figure 9b). The noise in the stress measurements (1σ standard deviation is $\sim$2 MPa) approaches the stresses being measured (3–4 MPa). The raw data were collected at a rate of 600 samples s^{-1} and 1000 samples were averaged to yield each individual data point in Figure 9a. There are several factors that contribute to the noise including analog-digital conversion, radio-frequency signals generated by SCR, and fluctuations or "dithering" of the servo-hydraulic drive. The differential piston stress prior to deformation increased slightly (0.018 MPa μm^{-1}) as the piston was advanced. In this particular experiment, the smoothed data were corrected for this increase in stress by second-order polynomial least-squares fitting of the stress-displacement data up to the hit-point and extrapolating that fit to the final displacement (Figure 9c). The deformation is assumed to be a homogeneous, constant-volume, uniaxial shortening (an excellent approximation in most cases), and the consequent increase in the cross-sectional area of the specimen is used for calculation of the specimen stress (Figure 9c). The resulting stress-strain curve for this experiment is shown in Figure 9d.

After the specimen is removed from the pressure assembly, the Pt capsule is removed, and the final dimensions of the specimen are carefully measured and compared for any discrepancies to those calculated by the stress-strain data

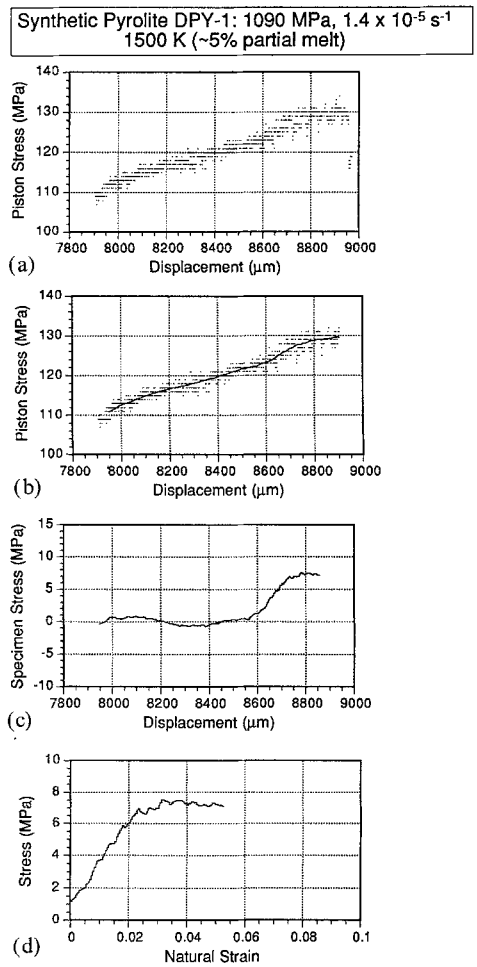

Figure 9

Stress-displacement record for deformation of a partially molten synthetic pyrolite polycrystal at 1090 MPa, 1500 K ($\sim$5% partial melt), at a strain rate of 1.4×10^{-5} s^{-1} (experiment GB40). The raw data are shown in (a) and smoothed data (100 point averaging) are shown in (b). (c) The smoothed data were corrected for friction by fitting the differential piston stress prior to the hit-point (8621 μm) to a second-order polynomial, and the differential piston stress was converted to specimen stress as described in the text. (d) The resultant stress-strain curve.

reduction. In cases where discrepancies are noted, it is possible to recalculate the stress-strain data using the measured final dimensions of the specimen. In general, such discrepancies introduce only minor errors to the measured flow stresses ($<10\%$).

For specimens with strengths greater than about 20–50 MPa, data reduction is more straightforward. Figure 10a shows the stress-displacement record for defor-

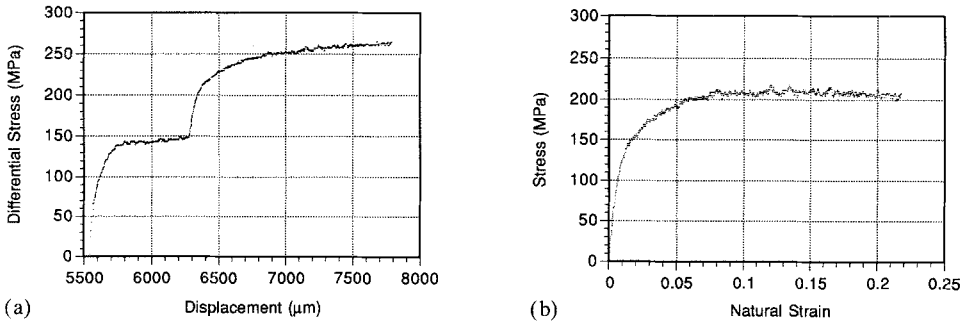

Figure 10
Stress-displacement record for deformation of Mg_2GeO_4 olivine polycrystal at 822 MPa, 1400 K at a strain rate of $4.5 \times 10^{-5}\ s^{-1}$ (experiment GB65). The raw data are shown in (a). The resultant stress-strain curve in (b) was calculated as described in the text.

mation of a Mg_2GeO_4 olivine polycrystal (see Figure 1, TINGLE *et al.*, 1993) at 822 MPa confining pressure, 1400 K at a strain rate of $4.5 \times 10^{-5}\ s^{-1}$ (experiment GB69). A zeroth hit was performed at the same conditions to 7% natural strain. The subsequent hit thus exhibited a sharp hit-point and a steep elastic slope (Figure 10a) as expected. The specimen flowed at a stress of 207 ± 4 MPa (the error is the 1σ standard deviation of the measured steady-state flow stress) to 22% natural strain. The stress-strain curve in Figure 10b was calculated using the measured initial dimensions of the specimen without smoothing or correcting the raw data for any time-dependence of friction. The steady-state flow stress calculated using the final specimen dimensions was 208 MPa, in excellent agreement with that obtained using the initial dimensions.

Measurement of Acoustic Emissions at High Pressure and Temperature

To measure acoustic emissions inside the pressure assembly, a miniature piezoelectric transducer ("pinducer") was spring-loaded against the bottom of the WC base anvil of the pressure assembly (Figure 2d). The pinducers are 2 mm diameter (Valpey-Fisher model VP1093) with a frequency response (-3 db) of 1.2 MHz and are high-pass filtered to have sensitivity in the range 0.2–5 MHz. The WC base anvil serves as an electrical lead for the graphite furnace, so the pinducer was insulated electrically by bonding a thin disk of alumina (~ 1 mm thick, polished flat and parallel) to its tip with silver-impregnated epoxy (probably any bonding agent will suffice). The pinducer was inserted through a 3 mm diameter hole in the WC insert in the base plate of the apparatus (Figure 1) and was electrically insulated from the base plate by wrapping the pinducer with a single layer of Scotch Transparent® tape (a number of other methods, paints, coatings, and teflon tape proved unreliable). Below the base plate, the shims and lower platen of the

apparatus were designed with 6.35 mm diameter concentric holes through which the feedthrough for the pinducer was passed (Figure 1). The feedthrough was surrounded by a sintered alumina tube for further electrical isolation.

The output of the pinducer was amplified 40–60 db (via a Panametrics 5660B battery-operated preamplifier) and input to discrimination and counting electronics (designed by C. Sondergal and fabricated by TAK at LDEO) and to a Tektronix model 2211 digital oscilloscope to store waveforms of individual acoustic events. The trigger level of the discriminator was tuned to be just above the electrical noise of the apparatus, so that the combined acoustic and electrical noise was about 3–4 counts min^{-1}. The counting electronics were set so that each event detected incremented the output voltage by $\sim$10 mV (1024 events equaled 10 Vdc). This voltage was input through an OM3 signal conditioner to the computer and stored on disk.

The measurement of acoustic emissions (AE) generated at high pressure and temperature was attempted as a part of ongoing investigations of the high-pressure faulting behavior of Mg_2GeO_4 olivine and its implications for the mechanism of deep earthquakes (e.g., GREEN and BURNLEY, 1989, 1990; BURNLEY *et al.*, 1991). Those results have been reported by GREEN *et al.* (1992) and TINGLE *et al.* (1993) and are briefly discussed here to illustrate the technique.

Acoustic events were monitored continuously during the experiments. During pressurization to 600 MPa, AE events typically were abundant, due most likely to compaction of the components of the pressure assemblies. Above 600 MPa during pressurization, AE was still observed but was relatively less frequent. After achieving a confining pressure approximately 150–200 MPa below the intended pressure of the experiment, the temperature was ramped to 900–1200 K at 5–10 K min^{-1}; AE events were observed at a low rate as during pressurization above 600 MPa, probably due to differential thermal expansion and continued compaction of the pressure assembly. After reaching the desired temperature and pressure, AE reached a stable level that was typically 3–4 counts min^{-1}. During piston advance, the AE remained at background levels. In some experiments, the piston was advancing through solid NaCl; the absence of any AE above background indicates that the NaCl flowed ductilely around the advancing piston. In others, the alumina piston was placed in contact with the specimen, and the WC piston advanced through Pb. No change in AE rate was observed during loading of the specimens until the stress drop associated with the high-pressure faulting was observed. During the stress drop, a burst of AE occurs which has been interpreted to be due to accelerations within the thin superplastic layer generated during nucleation and growth of the fault (TINGLE *et al.*, 1993). Lack of AE before the onset of failure demonstrates that the high-pressure faulting is not a brittle phenomenon. Some AE during the stress drop could be due to microfracturing associated with the dynamic mechanical instability, although microstructural evidence to support this has not been observed. After rupture, some specimens were allowed to slide along the fault and it was

noted that the AE diminished to levels only slightly above those recorded prior to failure, indicating that microfracture and comminution of grains in the faults as occurs during brittle sliding does not occur in specimens that have failed by the high-pressure faulting mechanism.

The digital oscilloscope was used to record individual acoustic events (see Figure 4, TINGLE *et al.*, 1993). Unfortunately, it was not possible to collect and analyze a large number of events with a single digital oscilloscope, because the storage capacity of the oscilloscope was limited and the data had to be transferred to another computer before a new waveform could be acquired. In the future, high-speed signal digitizers will be used to characterize the waveforms of the AE associated with the high-pressure faulting mechanism. The waveforms observed to date suggest that there may be two distinct populations of AE; the first population is impulsive and exhibits exponential decay, as is typical of brittle AE. The second population is not impulsive; the frequency of these events is strikingly monotonic, but the rise and decay envelope is asymmetric.

Summary

The techniques and equipment described here for experimental rock deformation at high pressures and temperatures are being used to address several important geophysical problems, among them the mechanism of deep-focus earthquakes, the rheology of partially molten rock and segregation of partial melt, the effects of nonhydrostatic stress on the kinetics of phase transformations, and the rheology of the upper mantle, transition zone, and the lower mantle as elucidated by the study of analogs to deep-mantle phases. The validity of such measurements has been established, and such measurements provide important constraints for geophysical models that attempt to describe dynamic processes in the Earth's interior. There is every reason to expect that techniques and apparatus for high-pressure rock deformation will continue to improve.

Acknowledgements

Various aspects of these developments have been supported by NSF Grants INT83–03077, EAR85–11809, EAR89–05059, EAR89–15938, OCE90–12941, EAR92–19369, and DOE grant GO3–88ER45360. We owe a special debt to J. Abril for design, fabrication, and maintenance of many components of the high-pressure apparatus and equipment used in this laboratory. We would like to thank M. Van de Water for TIG-welding the Pt capsules. P. Waterstraat has been an invaluable source of knowledge and help in automating and computer-interfacing the various electronic components of the high-pressure apparatus. The following

individuals have contributed ideas or designs that have led to our current apparatus and procedures: L. Anderson, R. S. Borch, P. M. Burnley, I. C. Getting, and P. Vaughan. M. Kanzaki and R. W. Luth shared information about interfacing the temperature controller to the computer. The philosophy underlying the development of this apparatus has been influenced by discussions over many years between HWG and Ed Schreiber, who was a good friend and stimulating colleague. He will be sorely missed.

REFERENCES

BORCH, R. S., and GREEN, H. W. (1989), *Deformation of Peridotite at High Pressure in a New Molten Salt Cell: Comparison of Traditional and Homologous Temperature Treatments*, Phys. Earth Planet. Int. *55*, 269–276.

BURNLEY, P. C., GREEN, H. W., II, and PRIOR, D. J. (1991), *Faulting Associated with the Olivine to Spinel Transformation in Mg_2GeO_4 and Its Implications for Deep-focus Earthquakes*, J. Geophys. Res. *96*, 425–443.

BUSSOD, G. Y., KATSURA, T., and RUBIE, D. C. (1992), *A New Method to Experimentally Determine the Rheologic Properties of Transition Zone Minerals at High P-T*, EOS, Trans. Amer. Geophys. Union *73*, 556.

CLARK, S. P. (1959), *Effect of Pressure on the Melting Points of Eight Alkali Halides*, J. Chem. Phys. *31*, 1526–1531.

CRC Handbook of Chemistry and Physics (R. C. Weast and M. J. Astle, eds.) 63rd edition (CRC Press, Boca Raton, Florida 1984).

CRC Handbook of Materials Science (C. T. Lynch, ed.) vol. II, *Metals, Composites, and Refractory Materials* (CRC Press, Boca Raton, Florida 1980).

DEVRIES, R. C. (1964), *The System Al_2SiO_5 at High Temperatures and Pressures*, J. Am. Ceram. Soc. *47*, 230–237.

GLEASON, G. C., and TULLIS, J. (1993), *Improving Flow Laws and Piezometers for Quartz and Feldspar Aggregates*, Geophys. Res. Letters *20*, 2111–2114.

GLEASON, G. C., and TULLIS, J. (1992), *Use of Molten Salt Cell for Experimental Deformation of Quartz and Feldspar: Preliminary Results*, EOS, Trans. Am. Geophys. Union *73*, 556.

GREEN, H. W. (1992), *Accurate Stress Measurement at Pressures to 5 GPa*, EOS, Trans. Am. Geophys. Union *73*, 556.

GREEN, H. W., and BORCH, R. S. (1989), *A New Molten Salt Cell for Precision Stress Measurement at High Pressure*, Eur. J. Mineral *1*, 213–219.

GREEN, H. W., and BORCH, R. S., *High pressure and temperature deformation in a liquid confining medium.* In *The Brittle-ductile Transition in Rocks, The Heard Volume*, Geophys. Monog. Ser. *56* (eds. Duba, A., Durham, W. B., Handin, J., Logan, J., and Wang, H.) (American Geophysical Union, Washington, D.C. 1990) pp. 195–200.

GREEN, H. W., and BURNLEY, P. C. (1989), *A New, Self-organizing, Mechanism for Deep-focus Earthquakes*, Nature *341*, 733–737.

GREEN, H. W., and BURNLEY, P. C. (1990), *The failure mechanism for deep-focus earthquakes.* In *Deformation Mechanisms, Rheology and Tectonics* (eds. Knipe, R. J., and Rutter, E. H.), Geol. Soc. London Spec. Pub. *54*, 133–141.

GREEN, H. W., and WALKER, D., *The multianvil as a deformation apparatus.* In *Proc. of the 29th Int. Geol. Congress* (August 1992).

GREEN, H. W., II, YOUNG, T. W., WALKER, D., and SCHOLZ, C. H. (1990), *Anticrack-associated Faulting at Very High Pressure in National Olivine*, Nature *348*, 720–722.

GREEN, H. W., II, SCHOLZ, C. H., TINGLE, T. N., YOUNG, T. E., and KOCZYNSKI, T. A. (1992), *Acoustic Emissions Produced by Anticrack Faulting During the Olivine → Spinel Transformation*, Geophys. Res. Letters *19*, 789–792.

HASKELL, R. W., and DEVRIES, R. C. (1964), *Estimate of Free Energy of Formation of Kyanite*, J. Am. Ceram. Soc. *47*, 202–203.

HOLLAND, T. J. B. (1980), *The Reaction Albite = Jadeite + Quartz Determined Experimentally in the Range 600–1200°C*, Am. Mineral. *65*, 129–134.

JOHANNES, W., BELL, P. M., BOETTCHER, A. L., CHIPMAN, D. W., HAYS, J. F., MAO, H. K., NEWTON, R. C., and SEIFERT, F. (1971), *An Interlaboratory Comparison of Piston Cylinder Calibration Using the Albite-breakdown Reaction*, Contrib. Mineral. Petrol. *32*, 24–38.

KANZAKI, M. (1990), *Thermal-analysis in a Multianvil High-P Apparatus*, EOS, Trans. Am. Geophys. Union *71*, 1697.

KERRICK, D. M. (1968), *Experiments on the Upper Stability Limit of Pyrophyllite at 1.8 kb and 3.9 kb Water Pressure*, Am. J. Sci. *266*, 204–214.

LEVIN, E. M., ROBBINS, C. R., and MCMURDIE, H. F., *Phase Diagrams for Ceramists 1969 Supplement* (American Ceramic Society, Columbus, Ohio 1969).

MEADE, C., and JEANLOZ, R. (1990), *Deep-focus Earthquakes and Recycling of Water into the Earth's Mantle*, *Science 252*, 68–72.

MEADE, C., and JEANLOZ, R. (1991), *The Strength of Mantle Silicates at High Pressures and Room Temperature: Implications for the Viscosity of the Mantle*, Nature *348*, 533–535.

MEAGHER, S., BORCH, R. S., GROZA, J., MUKHERJEE, A. K., and GREEN, H. W. (1992), *Activation Parameters for High-temperature Creep in Polycrystalline Nickel at Ambient and High Pressures*, Acta Metal. Material. *40*, 159–166.

MIRWALD, P. W., GETTING, I. C., and KENNEDY, G. C. (1975), *Low-friction Cell for Piston-cylinder High-pressure Apparatus*, J. Geophys. Res. *80*, 1519–1525.

SCHOLTZ, C. J., and KOCZYNSKI, T. A. (1979), *Dilatancy Anisotropy and the Response of Rock to Large Cyclic Loads*, J. Geophys. Res. *84*, 5525–5534.

TINGLE, T. N., GREEN, H. W., II, SCHOLZ, C. H., and KOCZYNSKI, T. A. (1993), *The Rheology of Faults Triggered by the Olivine-spinel Transformation in Mg_2GeO_4 and Its Implications for the Mechanism of Deep-focus Earthquakes*, J. Struct. Geol. *15*, 1249–1256.

WEIDNER, D. J., WANG, Y., and VAUGHAN, M. T. (1992), *X-ray Strain Measurement and Strength of Materials at High Pressure and Temperature*, EOS, Trans. Am. Geophys. Union *73*, 556.

WU, T.-C., BASSETT, W. A., BURNLEY, P. C., and WEATHERS, M. S. (1993), *Shear-promoted Phase Transitions in Fe_2SiO_4 and Mg_2SiO_4 and the Mechanism of Deep Earthquakes*, J. Geophys. Res. *98*, 19767–19776.

(Received April 2, 1993, revised October 5, 1993, accepted October 19, 1993)